SUPPLEMENT TO THE *WELDING JOURNAL*, FEBRUARY 2010
Sponsored by the American Welding Society and the Welding Research Council

Characterization of Welding Fume Generated by High-Mn Consumables

Fume particle size and mass distribution, phase identification, and composition for high-Mn welding consumables are reported

BY M. J. GONSER, J. C. LIPPOLD, D. W. DICKINSON, J. W. SOWARDS, AND A. J. RAMIREZ

ABSTRACT

The welding fume generated by two high-Mn hardfacing welding electrodes was evaluated using a range of fume collection and characterization techniques. This study included a shielded metal arc welding (SMAW) electrode and a flux-cored arc welding (FCAW) electrode both manufactured by Lincoln Electric Co. Data collected previously using an E6010 SMAW electrode were used for comparison. The fume generation rates under nominal welding conditions were relatively high, averaging 0.84 and 3.1 g/min for the SMAW and FCAW electrodes, respectively. Fume particle size and mass distribution were determined using an electrical low-pressure impactor (ELPI). This technique showed that the largest number fraction of fume particles for both electrodes was in the fine (0.1–2.5 μm) and ultrafine (< 0.1 μm) particle size regimes, while the largest mass fraction of fume particles was in the fine regime.

X-ray diffraction (XRD) analysis of bulk fume particles identified strong peaks for Fe_3O_4, $MnFe_2O_4$, and $FeMn_2O_4$ in the SMAW fume, while strong peaks for Fe_3O_4, $MnFe_2O_4$, and smaller peaks for CaF_2 and NaF were identified in the FCAW fume. Morphologically, the fume particles were typically spherical, present either as individual particles or multiparticle agglomerates. The SMAW fume particles contained high levels of Fe and Mn and suggested that Mn substitutes for Fe in the Fe_3O_4 lattice, resulting in Mn:Fe_3O_4 (Mn doped magnetite) having the same crystal structure as magnetite.

Analysis of individual fume particles and agglomerates using X-ray energy-dispersive spectroscopy (XEDS) in conjunction with transmission electron microscopy (TEM) revealed that the SMAW fume contained Fe, Mn, Mg, Si, Na, F, and O. The only phase that was unequivocally identified by selected area diffraction (SAD) in the TEM was Mn:Fe_3O_4. Agglomerates consisting of many small particles (10 to 30 nm) analyzed by SAD were shown to have an Fe-rich Mn:Fe_3O_4 crystal structure. TEM analysis of the FCAW fume revealed two basic types of fume particles. Most of the particles were roughly spherical with diameters ranging from 100 to 200 nm, while some were in the form of agglomerates of very small particles (Fe_3O_4) with diameters from 10 to 50 nm. SAD was used to identify individual square particles (~150 nm) as Mn:Fe_3O_4. X-ray photoelectron spectroscopy (XPS) was used to analyze the fume particle surface chemistry and generate compositional depth profiles by a sputter etching technique. These results showed an increase in Fe and Mn concentration upon etching, suggesting that a thin shell of different composition than the bulk particle is present on the particle surface.

M. J. GONSER (gonser.7@osu.edu), *J. C. LIPPOLD, and D. W. DICKINSON are with Welding & Joining Metallurgy Group, The Ohio State University, Columbus, Ohio. J. W. SOWARDS is with National Institute of Standards and Technology, Boulder, Colo. A. J. RAMIREZ is with Brazilian Synchrotron Light Laboratory, Campinas, SP, Brazil.*

KEYWORDS

Hardfacing Consumable
High-Mn Electrodes
Welding Fume
Fume Generation
FCAW
SMAW

Introduction

Recently, the American Conference of Governmental Industrial Hygienists (ACGIH) reduced the threshold limit value (TLV) for Mn particulate matter from 1 to 0.2 mg/m^3. The TLV reduction arose out of concern that increased Mn exposure may play a role in certain neurodegenerative diseases. Much debate surrounds the effect of Mn (or Mn compounds) in welding fume on the human body. The following statement has been issued by the International Institute of Welding (IIW) on Mn in welding fume: "There is no convincing evidence that exposure to manganese-containing fume during employment as a welder can result in an increased risk of developing neurobehavioral deficiencies and loss of motor skills. There is, however, insufficient evidence to the contrary to dismiss the possibility with absolute certainty" (Ref. 1). The goal of this investigation is to provide basic information on the nature of fume in two high-Mn, hardfacing consumables. While previous researchers have used a few selected techniques to study manganese in welding fume, this investigation has relied on a combination of fume collection and analytical techniques to provide a better "global" picture of the nature of welding fume. The details of these techniques and how they are applied to the study of welding fume were published previously by Sowards et al. (Refs. 2, 3).

A previous study has shown that high-Mn consumables may produce fume that contains between 1 and 15 percentage by weight (wt-%) of the total welding fume, compared to 6 wt-% Mn in mild steel consumables (Ref. 4). It has been shown that manganese in respirable fume particles is in the form of complex oxides (spinels), sometimes with a core-shell morphology where the particle core is surrounded by a silicon oxide shell (Ref. 5). The core is typically an Fe-rich oxide (Fe_3O_4) containing Mn, K, Cr, and O in

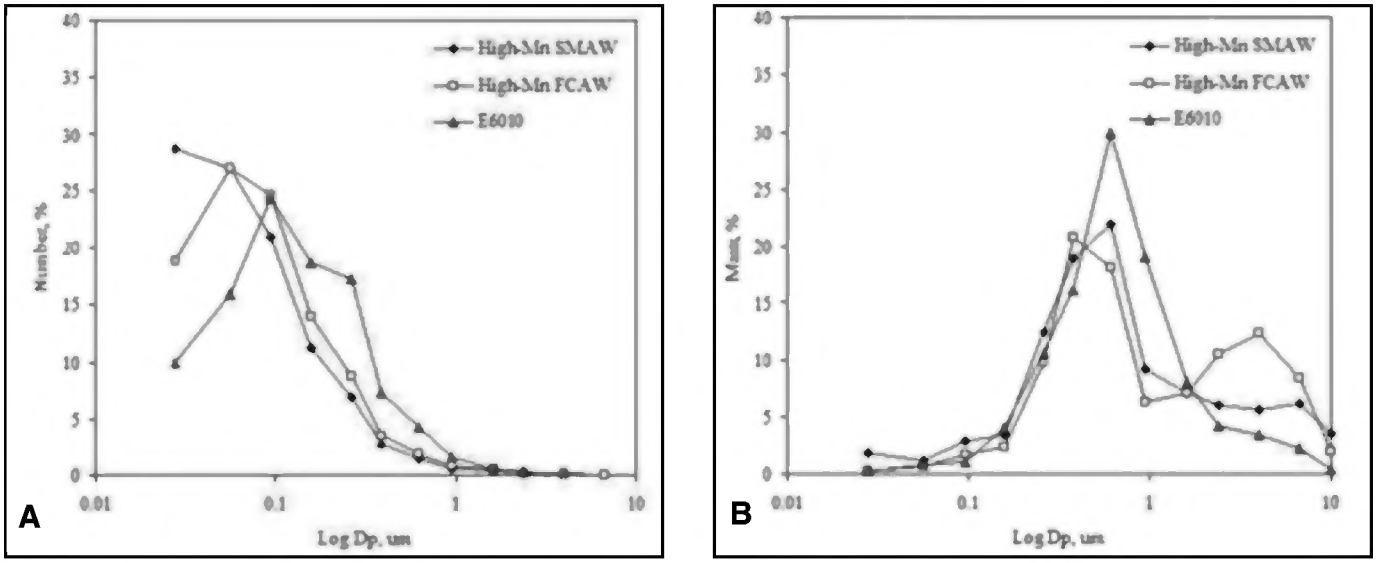

Fig. 1 — Distributions of high-Mn consumable fume and E6010 fume. A — Number; B — mass.

different ratios. The shell consists of silicon oxide and other compounds (fluorides) that result from additions to the SMAW electrode coating. In mild steel weld fume the predominant compound is magnetite — Fe_3O_4 (Ref. 6). Transition metals may substitute for iron in the magnetite lattice, but do not form in the pure oxide state (such as MnO_2) (Refs. 3, 7). In SMAW electrodes, Mn is the most common substitution due to its high concentration in the electrode coating. Minni et al. (Ref. 8) used XRD and XPS to determine that the oxidation state of Mn is primarily Mn^{-2} and Mn^{3+} for GMAW and SMAW, respectively. In the same study, XRD analysis of the SMAW fume showed that Mn was present in the fume as $MnFe_2O_4$ and $KMnO_2$.

Experimental Procedures

A "global" procedure for the evaluation of welding fume has previously been developed by Sowards et al. for the analysis of a wide range of welding consumables. The procedures used here are similar to those described in detail in a previous paper (Ref. 2).

Consumables

Two high-Mn hardfacing electrodes manufactured by The Lincoln Electric Co. were evaluated in this study. The consumables selected for this study were produced under the trademarks Wearshield Mangjet® (SMAW) and Lincore M® (FCAW). These electrodes are used to deposit weld metal that is highly resistant to wear and abrasion. The deposited weld metals are austenitic and can be work hardened by transformation to martensite to hardness levels in the range HRC 30–48. The nominal and actual deposit compositions of these consumables are listed in Table 1 along with the composition of the mild steel electrode E6010 that was used for comparison in this study.

Welding Procedures and Fume Collection

Nominal welding parameters were selected based on the manufacturer's rec-

Table 1 — Nominal and Actual Weld Metal Deposit Compositions

Elements (wt-%)	High-Mn SMAW(1)		High-Mn FCAW(2)		E6010	
	Nominal	Actual	Nominal	Actual	Nominal	Actual
Fe	Bal	Bal	Bal	Bal	Bal	Bal
Mn	14.5	10.2	13.0	9.4	0.45	0.55
Ni	—	0.077	0.5	0.56	—	0.048
Ti	—	0.013	—	0.11	—	—
Mo	1.15	1.1	—	0.018	—	0.018
Si	0.14	0.18	0.4	0.36	0.2	0.52
Cr	—	0.084	4.9	2.9	—	0.063
C	0.65	0.46	0.6	0.42	0.12	0.15
P	—	0.012	—	0.007	0.0075	<0.005
S	0.01	0.007	—	—	0.015	0.017
V	—	—	—	0.026	—	0.01
Cu	—	0.18	—	—	—	—
W	—	0.15	—	—	—	—
Al	—	—	—	0.032	—	—

(1) Lincoln Electric Wearshield Mangjet®, (2) Lincoln Electric Lincore M®

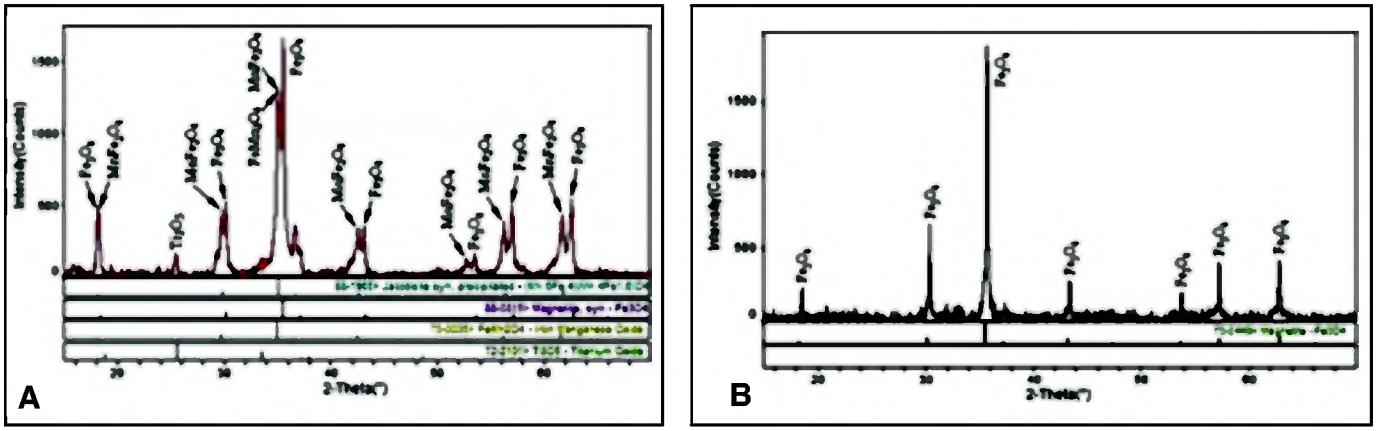

Fig. 2 — X-ray diffraction spectrum. A — High-Mn SMAW fume; B — E6010 (Ref. 3).

ommendation and represented the median parameters for the range provided. The actual welding parameters used in this investigation are provided in Table 2. All welds were deposited on plain carbon A36 steel plate. Fume was collected using both a modified AWS F1.2:1999 type fume hood and an electrical low-pressure impactor (ELPI). The ELPI sorts fume particles into 13 size ranges from 0.03 to >10 μm. Number and mass distribution analysis of the fume was conducted using the ELPI, while fume generation rates were determined using the AWS procedure. Fume collection procedure details are provided in Table 3. A minimum of three runs were conducted for each consumable in order to develop statistically valid data for fume generation rates, and particle number and size distributions.

Table 2 — Welding Parameters

Welding Parameters	High-Mn FCAW	High-Mn SMAW	E6010
Average current, A	269	157	115
Average voltage, V	26.2	18.8	30.8
Wire feed speed, in./min (mm/s)	170 (72)	—	—
Travel speed, in./min (mm/s)	10.6 (4.5)	10.25 (4.3)	11.1 (4.7)
Calculated heat input, kJ/in. (kJ/mm)	40 (1.6)	17.2 (0.68)	19.1 (0.75)
Electrode diameter, in. (mm)	5/64 (2)	5/32 (4)	1/8 (3.2)
Contact tip-to-work distance, in. (mm)	1.25 (32)	—	—

Table 3 — Details of Welding Fume Collection

Analysis Technique	SMAW Collection Time, s	FCAW Collection Time, s	Collection Medium	Method
Number Distribution	20	15	ELPI, greased Al substrates	Inlet pressure of 100 mbar. Charger activated. Current range of 400,000 fA. Charger had to operate in the 5 kV range. The charger current was typically in the 1 μA range. Gravimetric balance used to measure fume before and after number distribution.
Mass Distribution	20	15	ELPI, greased Al substrates	
SEM/XEDS	20	20	ELPI, Al substrate Stage 2, 4, 8, 10	12 collection stages used for fume collection on aluminum substrates. SEM, XPS sample collection was done without charger. Inlet pressure of 100 mbar was used during fume collection.
XPS	20	20	ELPI, Al substrate Stage 3	
FGR	45	10	0.3 μm glass filter in fume hood	AWS F1.2:1999 type. 40 ft^3 initial flow rate. Manometer used to detect pressure drop across filter. 0.3 μm glass fiber filter used for sample collection. Welding stopped when the pressure dropped to 10 $ft^{3/min}$. The remaining fume would be extracted for 30 s.
XRD	50	20	0.3 μm glass filter in fume hood	
TEM (XEDS/SAD)	5	5	C-coated, Cu grid above arc	TEM grids were held at 3 and 6 in. above the arc. Collection times were approximately 5 s.

Fume Generation Rate

The fume hood was used to collect bulk fume used in the determination of fume

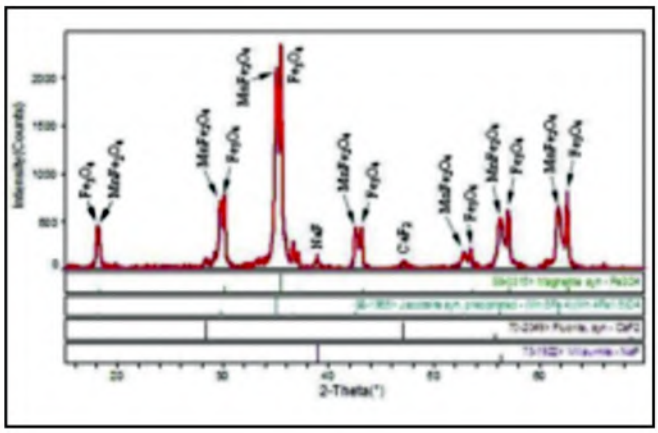

Fig. 3 — X-ray diffraction spectrum of high-Mn FCAW fume.

generation rate and for X-ray diffraction studies. The construction of the fume hood and fume generation tests were variants of the AWS F1.2:1999 specification. Instead of using a 4 μm cellulose fiber filter, glass fiber filters with an average pore size of 0.3 μm were used as a collection substrate in the fume hood. The smaller pore size was used to prevent any fume particle losses through the filter. (The backside of the filter was clean following testing.) Due to the smaller pore size, a 40 ft^3/min flow rate was required to get adequate flow through the filter. An automated rotary table was used to traverse the A36 steel plate under the electrode. A high-volume air sampling system (Model TFIA-F) was connected to the top port of the fume hood with a vinyl hose. The fume hood was equipped with a digital manometer so the pressure drop across the filter could be monitored. Fume was collected on the filter until the flow rate decreased to approximately 10 ft^3/min, after which the air pump would remain on for another 30 s. The filters for FGR and XRD analyses were stored in antistatic storage bags to avoid loss of fume from the substrate. Fume generation rate was determined by subtracting the initial weight from the final weight of the filter and dividing by the test time.

Particle Number and Size Distributions

A Dekati electrical low-pressure impactor (ELPI) was used to sample the welding fume. Similar to the FGR collections, a plate was traversed under the welding gun. Aluminum substrates were placed onto the individual impactor stages for fume collection. A 6-in.-diameter glass funnel was positioned 6 in. above the arc and attached to a 30-in. length of Tygon® tubing, with the other end of the tube connected to the inlet of the impactor column. TheTygon tubing had an outer diameter of ½ in., an inner diameter of ⅜ in. Once the charger and impactor column were assembled within the ELPI, a pressure of 100 mbar was applied using a Sogevac SV-25 vacuum pump with the flush pump on the ELPI activated. The flush pump was deactivated allowing the particles to be drawn toward the funnel, through the Tygon tubing, and into the unipolar charger. The charged particles then pass into a low-pressure impactor having electrically isolated collection stages. The particles collected on a specific impactor stage produce an electrical current that was recorded, in real time, by the appropriate electrometer channel. The ELPI classifies particles on 13 separate stages according to their aerodynamic diameter in the range of 0.03 to 10 μm.

Number distribution of the fume was determined using the ELPIV.1 software. Dekati collection substrate grease was applied to the surface of the substrates prior to being placed on the collection stages. This grease helps the particles to "stick" to the substrate during the collections process. Greased aluminum substrates were placed on the collection stages inside the ELPI. The current range used was 400,000 fA. Also, the charger was operated in the 5-kV range as this was the manufacturer's recommended charger voltage. The charger current was typically in the 1-μA range. Once the flush, pump, and charger were on, an "All-zero" calibration was performed to effectively zero the electrometers. This was done for each test run. Once the "All-zero" calibration had been completed, the flush would be turned off and the welding would be initiated using a remote control. Mass distributions were determined by weighing the aluminum collection substrates before and after testing using a gravimetric balance with precision of ±0.0001 g.

Characterization Techniques

Characterization techniques used in this study included X-ray diffraction (XRD), scanning electron microscopy (SEM), X-ray energy-dispersive spectroscopy (XEDS), X-ray photoelectron spectroscopy (XPS), transmission electron microscopy (TEM), and selected area diffraction (SAD). Details of these characterization techniques are listed in Table 4.

X-ray diffraction spectra were collected on fume particles collected on 0.3 μm filters in the bulk fume collection system. XRD data were used to determine which compounds were present in the fume. Data were collected using a Scintag XDS-2000 diffractometer equipped with a Cu X-ray tube and an energy-dispersive i-Ge detector. The goniometer was a vertical θ-θ arrangement in a standard Bragg-Brentano geometry. Several scans were performed after transferring the fume to a SiO_2 filter. The scans were run from 15 to 70 deg 2θ angles at a scan rate of 0.2 to 0.5 deg /min with the X-ray source running at 45 kV and 20 mA.

For SEM analysis, fume particles from Stages 2, 4, 8, and 10 of the ELPI were collected, representing average particle sizes of 0.06, 0.16, 0.96, and 2.4 μm, respectively. Grease was not applied to the aluminum substrates for the SEM collections due to the potential contamination. After ELPI collection, the aluminum foil would contain both discrete piles of fume particles and individual particles and agglomerates remote from the piles. SEM analysis was performed at the campus electron optics facility (CEOF) at The Ohio State University using a high-resolution scanning electron microscope, FEI Sirion, equipped with a field emission gun (FEG). This SEM has a microanalysis XEDS system, EDAX, equipped with a Si(Li) detector. Individual fume particles with diameters in excess of 3 μm were analyzed in the SEM. Analysis was performed at accelerating voltages in the range from 10 to 20 kV, and a pole piece to

Table 4 — Fume Characterization Details

Technique	Conditions
XRD	Cu X-ray source running at 45 kV and 20 mA. Scan from 15–70 deg 2θ angle. Rate of 0.2–0.5 deg/min.
SEM	15 kV, working distance of 5 mm. Collection time of 100 s for XEDS. Dead time in the range of 20–40%.
XPS	Pre-etch condition used to determine elements at surface of particles. Ar^+ ion etching reveals elements present at 5 nm depth in the particles.
TEM	300 kV. Collection time of 400 s for XEDS. SAD patterns.

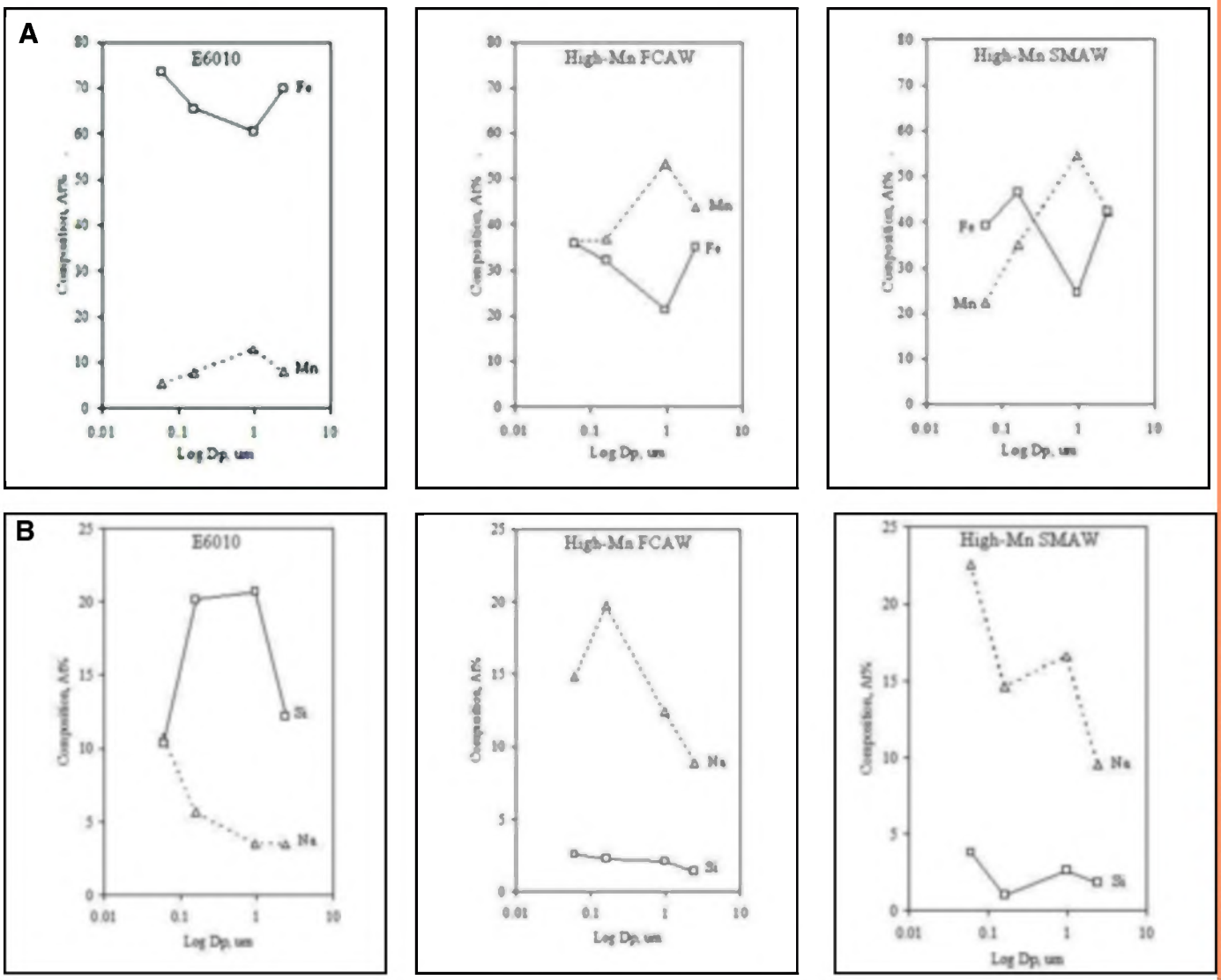

Fig. 4 — Bulk fume composition analysis (at.-%) taken from fume particle piles collected in the ELPI as a function of aerodynamic diameter for E6010, high-Mn SMAW, and high-Mn FCAW. A — Fe and Mn; B — Na and Si.

sample distance of 5 mm. Secondary electron images were collected of particles and agglomerates to determine the morphology of the fume. For the XEDS analysis, a spectrum collection time of 100 s was used. Dead time between 20 and 40% was utilized for composition analysis. Approximately 50 particles and agglomerates from each consumable were analyzed using XEDS. In addition, bulk fume pile composition was measured.

The XPS system used was a Kratos Ultra Axis XPS and UPS system with depth profiling capabilities using Ar^+ ion etching. In XPS, an X-ray is absorbed and a photoelectron is emitted. By subtracting both the energy of the impinging X-ray (which is known) and the energy of the electron (which is measured), the binding energy of the electron can be determined. Based on this information, the composition and valence states of various elements can be determined. Fume collected on stage 3 of the ELPI was used for XPS analysis. This stage represents a mean particle diameter of 0.095 μm. The charger inside the ELPI was deactivated during the collection of the fume for this analysis. Also, the aluminum substrate used in this test was not covered with collection grease.

The TEM samples were collected on carbon-coated 400 mesh TEM copper grids placed directly in the weld plume at approximately 3 in. above the arc. The TEM analysis was performed at the Brazilian synchrotron light laboratory (LNLS), using a JEOL HRTEM JEM 3010 URP instrument coupled with chemical nanoanalysis by XEDS equipped with a Si(Li) detector. A double-tilt beryllium sample holder was used for crystallographic and low background chemical analysis. TEM analysis was performed at 300 kV. For the microanalysis, probe sizes of 5 to 25 nm in diameter were used. The XEDS spectra were obtained with a dead time lower than 25%. In order to provide reliable statistics on the spectra collection, 400 s of collection time was used. Particles with sizes in the range of 10 to 300 nm were analyzed in the TEM. Bright field images were taken of the fume particles, while SAD was used to determine the crystal structure of the fume particles. Composition of the fume particles was determined using XEDS.

Results and Discussion

Fume Generation Rate

The fume generation rates for the high-Mn SMAW and FCAW consumables were 0.84 and 3.1 g/min, respectively. The FGR for the E6010 consumable was 0.60 g/min.

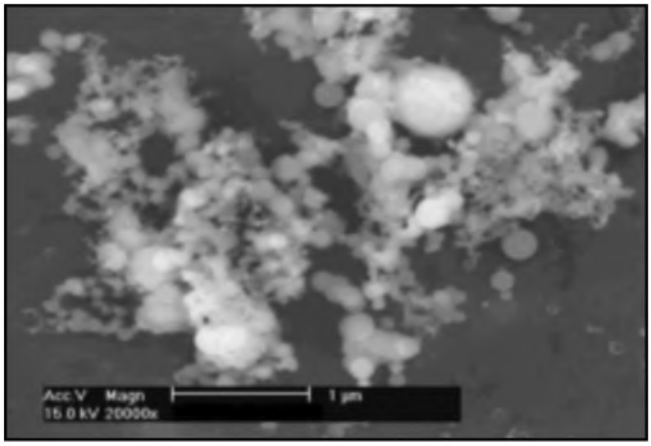

Fig. 5 — Scanning electron microscopy micrograph of high-Mn FCAW fume agglomerate.

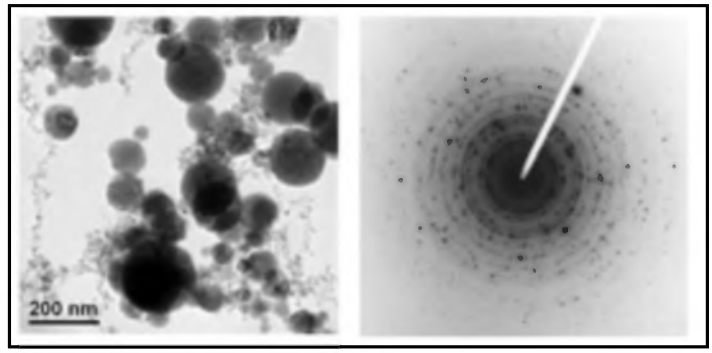

Fig. 6 — Fe-rich Mn:Fe_3O_4 particles as identified in high-Mn fume by SAD.

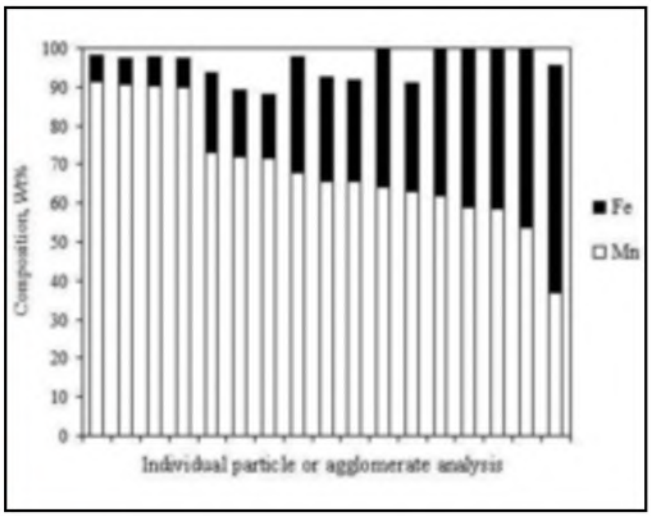

Fig. 7 — Fe and Mn composition of high-Mn SMAW paricles analyzed in the TEM. Oxygen was not included in this analysis. The remaining elements consisted of Na, Si, and Mg.

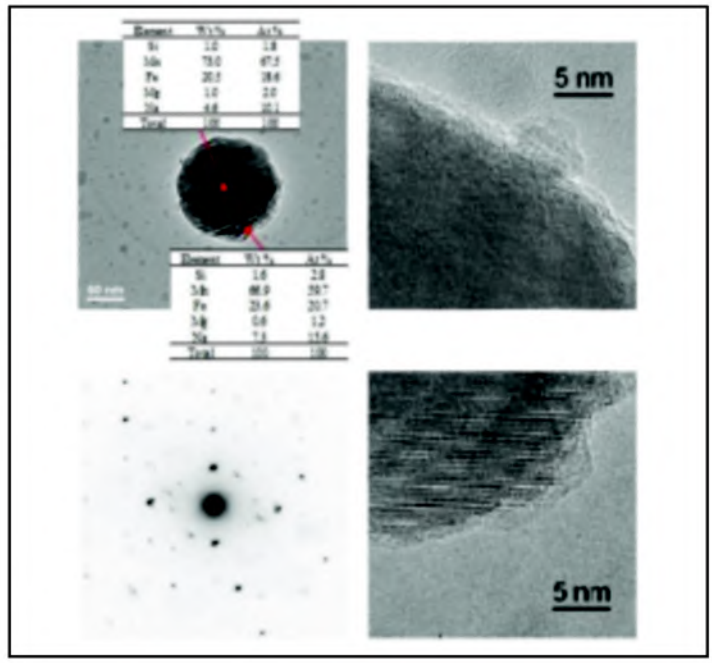

Fig. 8 — Medium-size Mn-rich Mn:Fe_3O_4 particles from high-Mn SMAW fume. The SAD pattern reveals a Mn:Fe_3O_4 structure. A core-shell structure with a very thin amorphous silicon oxide shell is present. Oxygen was not included in this analysis.

The high-Mn SMAW consumable had an FGR similar to that of E6010, but the FCAW had a significantly higher FGR, owing to the large quantity of the welding wire consumed. The higher fume generation rate of the high-Mn FCAW consumable is due to both the relatively high current levels (~270 A) at which this wire operates, and the fact that it is a self-shielded electrode.

Fume Particle Number Distribution

The results of the fume particle number distribution tests from the ELPI are provided in Fig. 1A. The majority of the fume particles were located in the fine (0.1–2.5μm) and ultrafine (< 0.1 μm) particle size regimes. This distribution is similar to E6010, except that E6010 had a slightly higher percentage of particles in the fine regime.

Mass Distribution

The results for the mass distribution tests are provided in Fig. 1B. The analysis shows that the majority of the mass of the particles for both the SMAW and FCAW electrodes is in the fine regime. This distribution is similar to other consumables that have been evaluated.

X-Ray Diffraction

The XRD spectrum for the high-Mn SMAW consumable is shown in Fig. 2A. Strong peaks were identified for Fe_3O_4 (magnetite) and $MnFe_2O_4$ (jacobsite). The iron dimanganese (III) oxide, $FeMn_2O_4$, was also detected. A reference spectrum for E6010 is shown in Fig. 2B. For this mild steel electrode, the only detectable compound is magnetite, Fe_3O_4.

The XRD spectrum for the FCAW consumable is shown in Fig. 3. This fume exhibited strong peaks for Fe_3O_4, $MnFe_2O_4$, and smaller peaks for CaF_2 (fluorite) and NaF (villiaumite). Based on SEM and TEM analyses presented in the following sections, some Mn substitutes for Fe in the Fe_3O_4 compound, resulting in Mn-doped magnetite (Mn:Fe_3O_4). This results in a slight shift in the peak relative to the Fe_3O_4 peak, but it still indexes as magnetite. In contrast, the E6010 bulk fume only exhibits peaks for Fe_3O_4 with small peak shifts suggesting the substitution of other elements (Mn, Si, and Na) for Fe (based on SEM and TEM results).

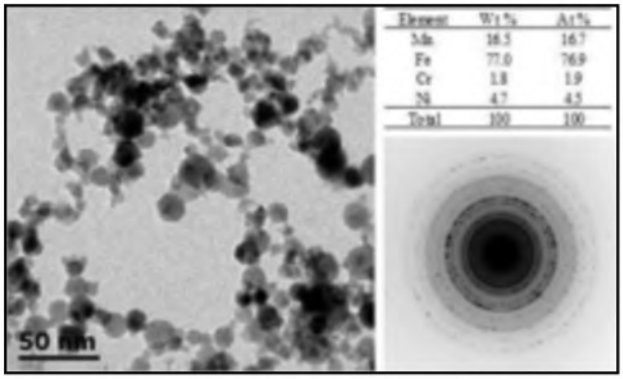

Fig. 9 — Small particle agglomerate from high-Mn FCAW fume that shows Fe_3O_4 type crystal structure. Oxygen was not included in this analysis.

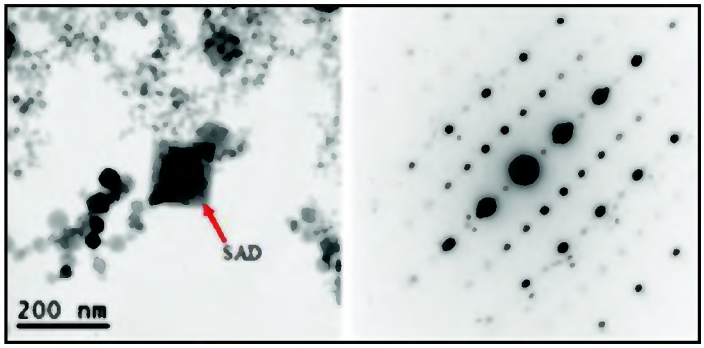

Fig. 10 — Large, square Mn:Fe_3O_4 fume particle from high-Mn FCAW. [013] zone axis.

Scanning Electron Microscopy

Morphological analysis revealed that the two high-Mn consumables produce similar fume types. The fume particles were typically spherical, either as individual particles or multiparticle agglomerates. Agglomerates collected on Stages 2 (0.06 μm) and 4 (0.16 μm) of the ELPI consisted of spherical particles. Agglomerates collected on Stage 8 (0.96 μm) consisted of larger spherical particles. The number of particles in the agglomerates on Stage 8 was considerably less than Stages 2 and 4. Stage 10 (2.4 μm) contained almost all individual spherical particles, which ranged in size from 0.5 to 3 μm in diameter. Very few agglomerates were collected on Stage 10 for both high-Mn consumables. The composition of the bulk fume piles collected in the ELPI for the three consumables is shown in Fig. 4. The Mn and Fe contents are shown in Fig. 4A, while Na and Si contents are shown in Fig. 4B.

The bulk fume analysis also revealed the presence of Mg, Mo, Ca, Ti, and Cu in the high-Mn SMAW fume, and Mg, Ca, Ti, and Cr in the high-Mn FCAW fume. The E6010 fume contained traces of Mg and Ti. Oxygen was detected in all of the fume particles, but was not quantified. Fluorine was detected in the high-Mn FCAW fume. This is consistent with the XRD results that showed the FCAW fume particles are comprised of metallic oxides and fluorides. The largest fraction of the composition for all of the fume particles consisted of Fe and Mn, with Na, Mg, Si, Ca, Ti, and Mo making up the difference. Table 5 shows the composition of the individual particles and agglomerates analyzed with XEDS in the SEM. These data present the average in atomic percent (at.-%) and standard deviation of the fume particle composition analyses.

The high-Mn SMAW fume exhibited an inverse compositional relationship between the Fe and Mn composition. When the Mn content was high, the Fe content was low. Conversely, when the Fe content was high, the Mn content was low. Nearly all of the fume particles, a total of nearly 50 individual particle analyses from the

Table 5 — Composition of Individual Fume Particles and Agglomerates for High-Mn and E6010 Fumes

		Elements (at.-%)							
<0.1 um	Value	Fe	Mn	Mo	Ti	Si	Na	Mg	Ca
High-Mn SMAW	AVG	50.4	26.5	3.2	—	4.8	8.8	6.4	—
	σ	10.8	11.6	2.2	—	2.0	5.6	3.8	—
High-Mn FCAW	AVG	34.7	24.6	4.9	3.3	1.9	17.3	14.8	2.2
	σ	11.7	11.7	4.1	2.4	0.9	5.5	5.0	1.0
E6010	AVG	76.7	11.6	—	—	6.5	4.8	—	—
0.1–1 um	Value	Fe	Mn	Mo	Ti	Si	Na	Mg	Ca
High-Mn SMAW	AVG	51.0	32.3	1.7	0.6	0.7	9.5	5.4	0.8
	σ	29.4	23.1	0.9		0.8	5.5	3.3	
High-Mn FCAW	AVG	20.1	47.1	3.0	1.5	1.1	12.6	14.5	1.2
	σ	17.3	19.7	2.4	0.8	0.9	3.1	9.3	0.7
E6010	AVG	71.6	8.7	—	—	15.1	3.6	0.4	0.5
>1 um	Value	Fe	Mn	Mo	Ti	Si	Na	Mg	Ca
High-Mn SMAW	AVG	51.2	32.4	0.5	1.3	2.4	9.8	5.8	1.0
	σ	28.9	23.8	0.3	1.7	1.5	5.8	0.9	0.9
High-Mn FCAW	AVG	47.3	32.4	2.9	2.2	1.0	7.5	3.7	1.1
	σ	23.4	19.9	1.5	0.7	0.5	4.9	2.7	0.4
E6010	AVG	58.1	8.7	0.5	12.5	14.2	2.3	—	2.1

Data are presented as average (AVG) and standard deviation (σ). Oxygen was detected, but not quantified in this analysis. Only AVG values were calculated for the E6010 consumable. Values are given in atomic percent (at.-%).

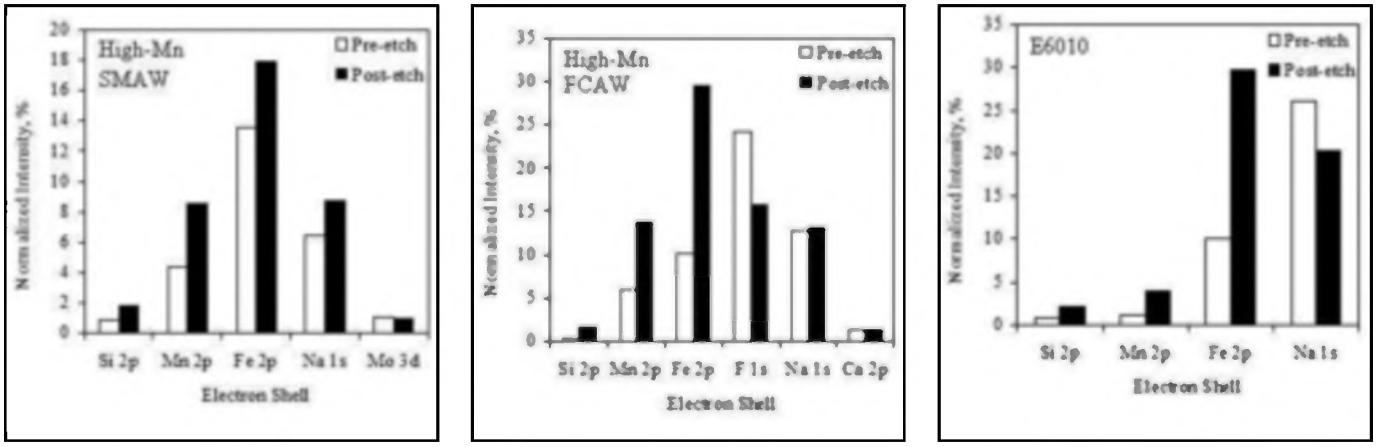

Fig. 11 — The XPS results for high-Mn SMAW (left), high-Mn FCAW (middle), and E6010 (right). Oxygen was detected but not included in these plots.

high-Mn-SMAW exhibited this type of behavior. For the high-Mn SMAW fume, Ca and Ti increased with particle diameter. Mo decreased with particle diameter. Na, Mg, Si, Mn, and Fe remained relatively constant with particle diameter. The high-Mn FCAW consumable contained about 6 at.-% Ni in some of the coarse (D_p > 1 μm) particles. Also, all of the size ranges for this consumable contained an average of 2 at.-% Cr. For the high-Mn FCAW consumable, Na, Mg, Si, and Ca appeared to decrease with particle diameter. However, this correlation takes into account the average composition of this size regime, and is not representative of all fume particles. The standard deviation values show that there is a wide variation in composition among these fume particles. Also, some of the fume particles that were analyzed were contained in agglomerates. An example of a high-Mn FCAW agglomerate is shown in Fig. 5.

The behavior of the E6010 consumable was different with respect to the Fe-Mn relationship. The Mn content of the E6010 electrode is fairly low compared to that of the high-Mn consumables, thus there is not as much Mn present in the fume. The E6010 particles were primarily Fe-rich oxides with Mn in the range from 8 to 12 at.-% and Si in the range from 5 to 20 at.-%. Some of the coarse particles contained about 12 at.-% potassium. When the Fe content of the E6010 fume particles decreases, there is no subsequent increase in Mn.

Transmission Electron Microscopy

Magnetite (Fe_3O_4), jacobsite ($MnFe_2O_4$), and iron dimanganese (III) oxide ($FeMn_2O_4$) have the same FCC crystal structure (space group 227) with slightly different lattice parameters. Therefore, differentiating between these three phases by SAD analysis is not possible. Thus, for simplicity, these three phases have been identified by SAD as Mn-doped magnetite, Mn:Fe_3O_4.

SMAW Particles

The elements detected by XEDS in the TEM analyses of the high-Mn, SMAW fume particles were Fe, Mn, Mg, Si, Na, F, and O. Fe, Mn, and O were the predominant elements detected in most particles. The only phase that was unequivocally identified by SAD in the TEM was Mn:Fe_3O_4 — Fig. 6. However, the presence of other compounds identified by XRD analysis, such as Mn-oxides, NaF and CaF_2, is suggested by the TEM analysis due to the observation of Mn-rich particles with low Fe and some F and Na revealed by the XEDS analyses. Some Si was also observed. Si was present in the form of an amorphous Si-rich oxide (SiO_2) forming as a "shell" on the particle surface. Small particle (10 to 30 nm) agglomerates analyzed by SAD were identified as Fe-rich Mn:Fe_3O_4. This fume also exhibited some medium size (30–70 nm) high-Mn oxides with a Fe_3O_4-like crystal structure. The presence of Na and the large Fe L_α peak observed suggested that F is present on these particles. It should be noted that the F K_α and Fe L_α peaks overlap, thus the F content is difficult to quantify by XEDS.

Not all the analyzed medium-size particles had a high Mn content. Some medium size and large particles (80–120 nm) had a high Fe content. A comparison of a range of particles in terms of Fe and Mn content as determined by XEDS is shown in Fig. 7. These crystalline oxides have been identified through SAD and high resolution TEM images as being Mn:Fe_3O_4. Some of the medium-size Mn-rich particles exhibited a very thin (1–2 nm) amorphous shell as shown in Fig. 8. This shell is a Si-rich oxide, as suggested by the large Si content at the particle surface. Among the analyzed medium-size and large Mn-rich particles, most of them were identified by SAD as Mn:Fe_3O_4. However, the identification of some of these high-Mn oxides was not possible.

FCAW Particles

The TEM analysis of the FCA welding fume revealed two basic types of fume particles. Most of the particles were roughly spherical with diameters between 100 and 200 nm. The second type consisted of agglomerates of very small particles with diameters between 10 and 50 nm. An agglomerate of spherical particles along with a corresponding SAD pattern and XEDS analysis is shown in Fig. 9. Some of the larger spherical particles show a very high Mn concentration at its core. SAD was used to identify individual square particles (~150 nm) as Mn:Fe_3O_4. Figure 10 shows a Mn:Fe_3O_4 particle with SAD pattern at the [013] zone axis. The larger fume particles contained mostly Fe, Mn, and O. However, Cr, Ca, Ti, F, Mg, and Si were also detected in some particles or regions of such particles (such as the outer shell). XRD and TEM-based chemical analyses detected the presence of fluorine compounds CaF_2 and NaF.

A large variation in the relative amounts of Mn and Fe was observed among the particles analyzed. For example, spherical particles, exhibited a 2:1 ratio of Mn to Fe. However, particles mostly consisting of Fe (with little Mn) or Mn (with little Fe) were also observed. On the other hand, most of the small-particle agglomerates that were analyzed were found to be Fe rich. In general, the small-particle agglomerates were Fe rich, with approximately 70–80 wt-% Fe and 15–20

wt-% Mn. The crystal structure of these agglomerated particles corresponded to Fe_3O_4, as determined by SAD.

The TEM analysis of the E6010 fume particles also showed evidence of a core-shell type morphology. Where the core was identified as Mn:Fe_3O_4 and the shell an amorphous Si-rich oxide. Therefore, this result is similar to the high-Mn SMAW fume presented here.

X-Ray Photoelectron Spectroscopy

XPS analysis was conducted both before and after etching using Ar-ion sputtering. The pre-etch condition detects elements present on the surface of the particles, while the post-etch condition reveals elements below the outer layer of the fume particles. Since many particles are evaluated simultaneously, the XPS results represent an average composition profile over many particles. The area of the intensity for elements of interest is plotted as counts per second (CPS). These intensities are normalized from the sum of the intensities for all elements for both the pre-etch and post-etch conditions. Figure 11 shows XPS results for the high-Mn consumables and the reference E6010 fume.

The XPS results from the high-Mn SMAW fume show that the metallic species Si, Mn, Fe, and Na increase in intensity below the surface. The results for the high-Mn FCAW fume also shows that Si, Mn, and Fe intensity increase below the surface of the particles. For the FCAW fume, the particle surface was enriched in F. Based on the XRD analysis (Fig. 3), it is probably present as a NaF or CaF_2 compound. Manganese was present as complex oxides, while the XPS data show that Fe was present, in part, as elemental Fe. For E6010, metallic species Fe, Mn, and Si increase as the surface layer is removed. The outer region of the E6010 particles were enriched in Na. For all of the fume types, oxygen intensity decreased by nearly half following Ar^+ etching. This suggests that the particle surfaces are heavily oxidized, in some cases due to the presence of a SiO_2 shell. The XPS analysis also suggested that the Mn oxidation states are Mn^{+2} and Mn^{+3} based on the energies of the observed 2p peaks.

Conclusions

1) The fume generation rates for the three consumables are as follows: high-Mn SMAW: 0.84 g/min, high-Mn FCAW: 3.1 g/min, and E6010: 0.60 g/min.

2) The fume particle number distribution revealed that more than 95% of the particles are in the fine (0.1–2.5 μm) and ultrafine (less than 100 nm) size regimes. The peak in fume particle mass is in the fine regime.

3. The XRD analysis of high-Mn SMAW fume showed strong diffraction peaks for magnetite (Fe_3O_4), most likely with Mn substituted for some of the iron in the magnetite, $MnFe_2O_4$, and $FeMn_2O_4$. The high-Mn FCAW fume contained a Fe_3O_4-type compound in addition to $MnFe_2O_4$. The fluoride compounds NaF and CaF_2 were also identified for the high-Mn FCAW fume.

4) The XEDS analysis in the SEM showed a wide composition range for the fume particles with most particles consisting of Fe, Mn, Na, Mg, and Si. Elements in the fume particles could be traced back to the consumable composition. For instance, the high-Mn FCAW consumable produced fume that contained Cr and Ni, while the other consumables did not.

5) The XEDS analysis of the high-Mn SMAW fume in the TEM showed that Fe, Mn, Si, Na, and Mg were the predominant elements observed in most particles. The only phase unequivocally identified by SAD in the TEM was Mn:Fe_3O_4.

6) The TEM analysis of the high-Mn FCAW fume shows that the large particles are generally Mn-rich and exhibited the Mn:Fe_3O_4 structure.

7) The XPS results from the high-Mn SMAW fume show that Si, Mn, Fe, and Na increase in intensity below the surface of the particles. The results for the high-Mn FCAW fume show that Si, Mn, and Fe intensity increase below the surface of the particles. The FCAW particle surfaces are rich in F.

8) Based on the combined characterization results, it can be concluded that Mn is present in either the Mn^{+2} or Mn^{+3} valence state. No free Mn or Mn-oxides were identified in any of the analyzed fumes.

Acknowledgments

This project was supported by D&L Welding Fume Analysis, LLC, that represents a consortium of past and present welding consumable manufacturers.

References

1. International Institute of Welding. 2006. *IIW Statement on Manganese*, Paris, France.

2. Sowards, J. W., Ramirez, A. J., Dickinson, D. W., and Lippold, J. C. 2008. Characterization procedure for the analysis of arc welding fume. *Welding Journal* 87(3): 76-s to 83-s.

3. Sowards, J. W., Lippold, J. C., Dickinson, D. W., and Ramirez, A. J. 2008. Characterization of welding fume from SMAW electrodes — Part I. *Welding Journal* 87(4): 106-s to 112-s.

4. Tandon, R. K., Ellis, J., and Crisp, P. T. 1986. Chemical investigation of welding fumes from hardfacing and HSLA steel electrodes. *Welding Journal* 65(9): 231-s to 236-s.

5. McMillan, G. 2005. Is electric arc welding linked to manganism or Parkinson's disease? *Toxicology Rev.*, 24(4), 237–257.

6. Jankovic, J. 2005. Searching for a relationship between manganese and welding and Parkinson's disease. *Neurology*, 64, 2021–2028.

7. American Welding Society. 1983. Characterization of arc welding fume. Miami, Fla., ISBN 0-87171-229-6.

8. Minni, E., Gustafsson, T. E., Kopenen, M., and Kalliomaki, P. 1984. A study of the chemical structure of particles in the welding fumes of mild and stainless steel. *Journal of Aerosol Science* 15(1),: 57–68.